J Membrane Biol (2015) 248:505–515
DOI 10.1007/s00232-014-9702-8

Structural and Thermodynamic Insight into Spontaneous Membrane-Translocating Peptides Across Model PC/PG Lipid Bilayers

Yuan Hu · Sandeep Patel

Received: 7 May 2014 / Accepted: 18 June 2014 / Published online: 10 July 2014

Abstract We present results of Martini coarse-grained force field simulations to estimate the potentials of mean force for a series of recently screened spontaneous membrane-translocating peptides, SMTPs. We consider model bilayer composed of POPC and POPG, the latter providing the anionic component as used in experimental studies. We observe a significant barrier for translocation in the case of the canonical cationic cell-penetrating peptide nona-arginine, ARG9. In the case of the TP1, TP2, and TP3 peptides, potentials of mean force are systematically lower relative to the ARG9 case. Though the barriers predicted by the simulations, on the order of 20 kcal/mol, are still rather large to recapitulate the experimental kinetics of internalization, we emphasize that the qualitative trend of reduction of barrier heights is a significant result. Decomposition of the PMFs indicates that though there is a substantial entropic stability when the peptides reside at bilayer center, barriers as predicted from these force field-based studies are largely determined by enthalpic (potential energy) interactions. We note that the binding of the SMTPs is critically dependent on the mix of hydrophilic and hydrophobic residues that constitute the amino acid motif/sequence of these peptides. For the cationic ARG9 which only contains hydrophilic residues, there is no tight binding observed. The specific motif ΦR$\Phi\Phi$R (where Φ is a general residue) is a potential sequence in drug/peptide design. The SMTPs with this motif are able to translocate into membrane at a significantly lower free energy cost, compared to the negative control peptides. Finally, we compare the different membrane perturbations induced by the presence of the different peptides in the bilayer center. In some cases, hydrophilic pores are observed to form, thus conferring stability to the internalized state. In other cases, SMTPs are associated only with membrane defects such as induced membrane curvature. These latter observations suggest some influence of membrane rigidity as embodied in the full range of membrane undulatory modes in defining pore-forming propensities in bilayers.

Keywords Spontaneous membrane-translocating peptides · Molecular dynamics simulations · Umbrella sampling · Nano-arginine · Lipid bilayer · Cell-penetrating peptides · Anionic lipid

Introduction

Though cellular membranes are commonly considered barriers between the cell cytoplasm and extracellular milieu, recent decades have brought to light a wide spectrum of species that are able to translocate through these membranes as well as through model lipid membranes (Green and Loewenstein 1988; Lundberg and Langel 2003; Zorko and Langel 2005; Järver and Langel 2006; Jiao et al. 2009; Pavan and Berti 2011; Saalik et al. 2011; Walrant et al. 2013; Shin et al. 2013; Bechara and Sagan 2013). The canonical HIV TAT and oligoarginine species have enjoyed a rich history in terms of the amount of research expended into understanding mechanisms related to the internalization of such molecules (Bechara and Sagan 2013). Major challenges toward mechanistic explanations have involved the need to resolve between energy-

Electronic supplementary material The online version of this article (doi:10.1007/s00232-014-9702-8) contains supplementary material, which is available to authorized users.

Y. Hu · S. Patel (✉)
Department of Chemistry and Biochemistry, University of Delaware, Newark, DE 19716, USA
e-mail: sapatel@udel.edu

dependent and diffusive processes of translocation (Schmidta et al. 2010). The former mechanism broadly encompasses processes involving various cellular machineries that facilitate incorporation of extracellular species (Bangel 2006). In this work, we consider cell-penetrating peptide translocation across model lipid bilayers in the context of a diffusive process where cellular, energy-dependent machinery is not involved. Here, we consider the free energetics of a new class of cell-penetrating peptides, SMTPs, that were recently identified using high-throughput, orthogonal screening assays (Marks et al. 2011; He et al. 2012). We use molecular dynamics (MD) simulations using the Martini Coarse-Grained Force Fields (Marrink et al. 2004; Yesylevskyy et al. 2010; Monticelli et al. 2008; DeJong et al. 2013) for lipids, proteins, water, and ions to estimate the free energy of translocation of these peptides from bulk aqueous-like environments to the bilayer center. Free energetics are embodied in potentials of mean force, vis-a-vis the reversible work associated with transfer of a peptide from bulk aqueous environment to bilayer center. In the context of diffusive processes, the potential of mean force is a natural thermodynamic entity to consider as it is directly related to process kinetics (though in this work, we will not address translocation kinetics directly). We will use umbrella sampling molecular dynamics simulations. Our aims are several. First, we explore the extent to which coarse-grained models can recapitulate experimental observations related to peptide translocation. At the very least, we seek to find trends demonstrating higher stability (or lower free energy barriers to translocation) for screened and/or designed peptides known to spontaneously partition into cells and bilayers. Second, based on simulation results, we hope to relate the direct interactions of specific residues of the chosen peptides with membrane components. This is important in understanding the roles of polar, charged, and hydrophobic residues in cell-penetrating peptides as has been recently suggested in the literature (Marks et al. 2011; Lin et al. 2012; He et al. 2012, 2013; Cruz et al. 2013). Third, we seek to understand if structural perturbations of the model bilayers we employ are correlated to estimated free energetics (stability, translocation barrier).

Method

Umbrella sampling (US) molecular dynamic simulations were carried out to study the translocation of Spontaneous Membrane-translocating Peptides (SMTP) or inactive control peptides through a 90:10 molar ratio of 2-oleoyl-1-pamlitoyl-sn-glyecro-3-phosphocholine (POPC) and 2-oleoyl-1-pamlitoyl-sn-glyecro-3-glycerol (POPG) mixture lipid bilayers. We used recently developed Martini Polarizable Coarse-Grained force field (Monticelli et al. 2008; DeJong et al. 2013; Yesylevskyy et al. 2010) to simulate the interactions between system components. We considered a fully hydrated POPC/POPG bilayer patch of 256 lipid molecules (128 lipids per leaflet), consisting of 26 POPG randomly mixed with 230 POPC molecules (13 POPG and 165 POPC per leaflet). 26 sodium ions are added to neutralize the negative charges on POPG. 7536 coarse-grained water molecules and 150 mM NaCl salt are used to solvate the lipid molecules. All the simulations were performed using MPI supported GROMACS software package (version 4.6.3).

The simulation cells consist of a rectangular box of dimensions around $9.13 \times 9.13 \times 14.90$ nm, yielding about a 2.1-nm thick slab of lipid molecules surrounded by bulk water and ions. We used a time step of 20 fs and updated the neighbor list every ten step. The Lennard–Jones (LJ) and electrostatic (Coulomb) interactions were calculated by using simple spherical cutoff at a distance of 1.2 nm with a smooth switching function of distances 0.9 and 0.0 nm, respectively. The relative dielectric constants were set to 2.5 for use with the polarizable water force fields. To maintain the temperature 310 K and a pressure of 1 atm for the systems, we used the Berendsen weak coupling scheme with time constants of τ_T = 1.0 ps and τ_P = 5.0 ps, respectively (Berendsen et al. 1984). To keep the bilayer in a tensionless state, periodic boundary conditions with a semi-isotropic pressure coupling algorithm with a 3.0×10^{-4} bar^{-1} compressibility were used. The LINCS algorithm (Hess et al. 1997) was used to apply the bond constraint present in Martini force fields.

The system was minimized using the steepest descent method, followed by an equilibration run at 1 atm pressure and 310 K for 1 μs in the NPT ensemble. During the MD equilibration, the area per lipid of POPC/POPG-mixed bilayer equilibrated to the values of 0.651 nm^2 (see SI Fig. S1).

To obtain a PMF for the transfer of peptide in each system, we run 61 umbrella sampling (US) windows that range from 0.0 to 6.0 nm at a spacing of 0.1 nm along our chosen order parameter (OP), which is z-dimension distance between the center of mass of the peptides and bilayer. We first considered generating initial configurations in the windows along the specified OP by growing a peptide in the bulk water of the above equilibrated systems and further equilibrating the peptide–bilayer–water–ion system for about 100 ns after growing in aqueous phase. In order to prevent unnecessary drift of membrane, a position restraint along z-dimension with a force constant of 1,000 kJ/mol/nm^2 was applied on the head group beads (NC3, GL0, PO4) of the lipid molecules during the growing-in phase for all the simulations. The growing of peptide inside the system was done in two steps. We first slowly raised the Lennard–Jones interactions up to normal

strength over the course of a 10-ns simulation period using the method of thermodynamic integration as implemented in GROMACS, where step length ($d\lambda$) is set to 2×10^{-6} per time step, and Soft-core potential was used to prevent bead overlap. In the following step, we slowly grew in the Coulomb interactions using the same protocol. Each window was simulated for about 300 ns, and the total simulation time period is about 18.6 ms. For US MD simulations, we applied harmonic potential with a force constant of $3,000$ kJ/mol/nm^2 to restrain the peptide at each window. The details of the window setup and US method have been described in detail in our recent work (Hu et al. 2014). The weighted histogram analysis method (WHAM) was used for postsimulation unbiasing of umbrella sampling data (Kumar et al. 1992).

Finally, we put peptide at bulk water (z-distance of 6.0 nm to the center of bilayer) and performed 1 μs MD simulation for each system without any restrain to study the binding between SMTP or control peptides and POPC/POPG bilayers.

Results and Discussion

Peptide Binding

Since binding of a peptide to the membrane–water interface is an essential mechanistic component of peptide translocation, we first address the nature of peptide binding to the model bilayer we study. We first comment on the case of ARG9. In agreement with experimental observations that there is no spontaneous translocation of ARG9 across lipid bilayers, there is growing consensus that ARG9 follows an endocytosis pathway for uptake into cells (Bangel 2006; Marks et al. 2011). There are very few ARG9 data in clean synthetic lipids/vesicles, and virtually none in cases where little to no anionic character is present in the lipid composition of the model bilayers to support a purely diffusive translocation mechanism for this highly charged cationic peptide. Cellular uptake profiles of most cationic CPPs such as ARG9 are dependent on CPP concentration, and almost no uptake of CPP takes place at concentrations below some threshold value (Tunnemann et al. 2009; Kosuge et al. 2008). Unlike the case of cationic CPPs, experiments indicate that SMTPs such as TP2 have a remarkable ability to spontaneously translate across membranes without disrupting them. Translocation occurs at low peptide:lipid ratio (1:6000) and still shows the same partition coefficient as at higher ratios (Marks et al. 2011; He et al. 2012), indicating translocation of a monomeric species.

SMTP	
TP1: PLIL-LRLLR-GQF	**+2**
TP2: PLIY-LRLLR-GQF	**+2**
TP3: RRIL-LQLLR-GQF	**+3**
Control	
ONEG: PLGR-PQLRR-GQF	**+3**
DNEG: DDIL-LQLLD-GQF	**-3**
ARG9: RRR-RRR-RRR	**+9**

Fig. 1 The sequences and charges of peptide studied. In this work, we looked at three spontaneous membrane-translocating peptides (TP1, TP2, TP3), and three control peptides (DNEG, ONEG, ARG9), identified in a high-throughput screen (Marks et al. 2011). For visualization, the sequences are separated by dashes into three segments

Almost all the SMTPs (such as TP1, TP2) contain a special consensus (or conserved) sequence motif ΦR$\Phi\Phi$R (Φ is hydrophobic residue, and R is arginine) (He et al. 2012), which is also found in the voltage-sensing S4-helix (see Fig. 1). It is suggested that the physical properties of this motif have a role in facilitating spontaneous translocation of SMTPs. It is important to note that replacing one arginine residue to glutamate in the motif still allows translocation, such as indicated for TP3. However, replacing both arginines will cause little or no translocation, such as observed with the sequence of DNEG. DNEG has identical hydrophobic residues and pattern as TP3 but all the cationic arginines are replaced with anionic aspartates. The free energy barrier of TP3 is 35 kcal/mol lower than the DNEG. The barrier is significantly reduced due to this specific motif. Experimentally, it is found that there is no spontaneous translocation for DNEG. Both the arginine and hydrophobic residues in this motif play an important role. In our free simulations, we observed that peptides with this motif can bind at the membrane–water interface. In Fig. 2, we show distributions of the minimum distance between each residue/bead of the peptide and any membrane bead. We find that the charged arginine residues always have a high probability to be closer to the membrane atoms (see top panels in Fig. 2). This is due to the strong electrostatic interactions between the positive charge of arginine and the anionic components of the lipid bilayer. We observe a similar behavior for glutamine (Q) which presents a partially positive nitrogen atom to the anionic components of the bilayer. We do not observe stable binding of ARG9 to the bilayer-water interface. This suggests that hydrophobic residues play an important role in peptide binding, as these residues reside deeper inside the bilayer once they bind to the membrane (see bottom panels in Fig. 2). In Fig. 2, we see that the absolute position of the residues of the SMTP peptides lies generally further into the bilayer compared to the residues of the control peptide sequences. The combination of hydrophobic and hydrophilic residues will provide the flexibility

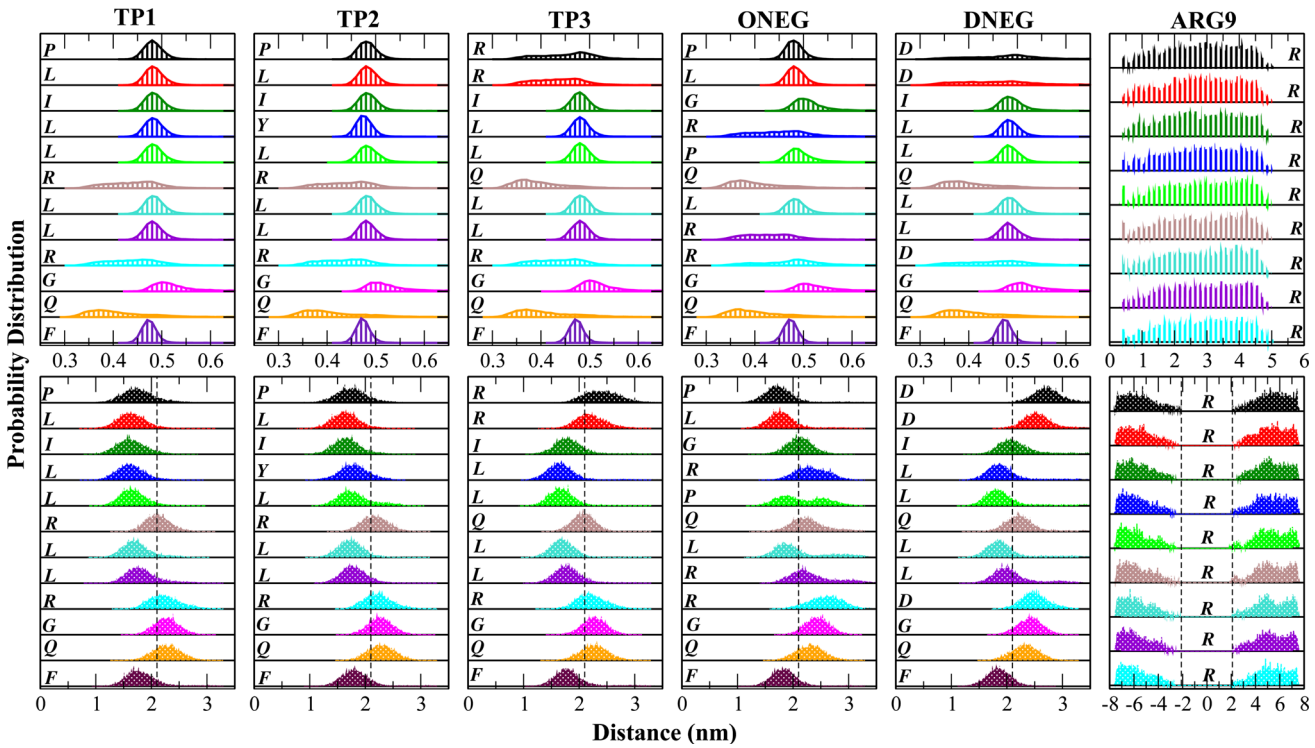

Fig. 2 (*top panels*) Probability distribution of the minimum distances between each residue of the peptide beads and POPC/POPG membrane beads, and (*bottom panels*) probability distribution of the distances between the center of mass of each residue of the peptide and the center of mass of POPC/POPG membrane in a 1 μs molecular dynamic simulation without restrain. The first 200 ns data are considered as the binding time, which are excluded from the distribution calculation of each peptide (trajectories can be found in SI Figs. S2–S5). *Vertical lines* (at +2.1 or −2.1 nm) in the *bottom panels* indicate the peak density of phosphates (see Fig. S6 in SI for more details of the density profile)

needed by the peptide to adapt configurations/conformations that allow it to optimally couple with the deformations of the membrane in order to confer some degree of overall free energetic stability (at least relatively higher than for the cases of the non-translocating control peptides and ARG9). Sequences of diverse types of amino acids lead to the hydrophobic residues locate inside, and hydrophilic residue come up to interact to head groups. Comparing ONEG with TP3, one hydrophobic residue leucine (L) was changed to arginine in the motif, and the barrier is increased by about 20 kcal/mol. This indicates that the spacing of arginine residues within the motif may play an important role. In Fig. 2, the RR sequence in ONEG places the arginines at two different depths in the bilayer, and only one residue maintains strong interactions with lipid phosphates. However, in the SMTPs, the arginine residues are ideally situated to interact with the headgroup, and the hydropobic residues reside closer to the membrane core, which can be stabilized by the lipid hydrocarbon tails. The relative position and separation of arginines reconciles the peptide with the lipid structures and may serve as the driving force of the peptide permeation into the center of the bilayer. We analyzed our simulations by counting the number of headgroup atoms, tail atoms, and ion/water atoms around each peptide residue in a shell of 0.67 nm radius (see Figs. S7–S12 in SI). We found that for hydrophilic residues arginine (R) and glutamine (Q), there are always more polar headgroup atoms, ions and water present compared to the less non-polar tail atoms. Also, the number of water and ions is always greater than headgroups. We monitor about 8–10 headgroup atoms and 10–20 water–ions. This suggest that the lipid headgroups and water ions maintain interactions with polar residues (R,Q) at all depths in the lipid bilayer. This strong interaction is one driving force for membrane deformation and pore formation (Freites et al. 2006; Schow et al. 2011).

Translocation Free Energy

Umbrella sampling potentials of mean force for each of the peptides introduced in the "Methods" section are shown in Fig. 3. The *x*-axis represents the z-component of the center of mass separation distance between the peptide and bilayer (our order parameter). A value of zero in the z-distance order parameter corresponds to the peptide at the center of the bilayer, and the value of 6 nm corresponds to the peptide in bulk solution.

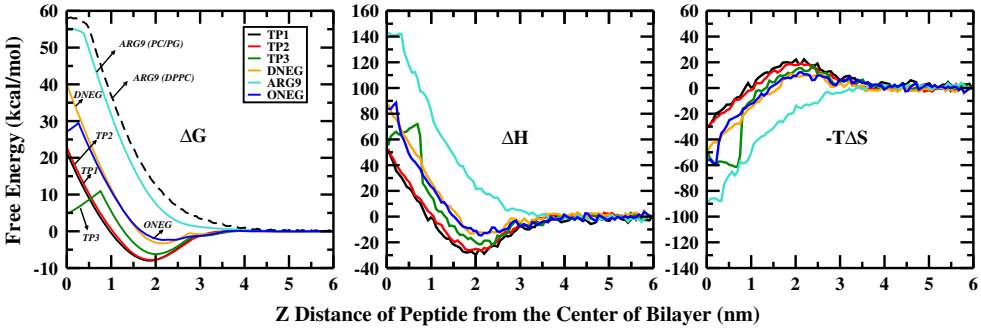

Fig. 3 Free energy ΔG, Enthalpic ΔH, and entropic-TΔS contributions to the total PMFs of translocating single peptide TP1, TP2, TP3, ONEG, DNEG, and ARG9 into the center of the model 90:10 POPC:POPG lipid bilayers

The PMFs of all the SMTP (TP1, TP2, TP3) are predicted to have lower translocation barriers to the center of the POPC/POPG bilayer relative to bulk aqueous solution than the control peptides (ONEG, DNEG, ARG9). The current force field and methodological combination predict that the free energy cost for transfer of SMTP is less than 23 kcal/mol. A recent study from Lazaridis et al. also obtained similar free energy magnitudes for TP2 using implicit membrane models in conjunction with free energy methods; the authors report a value of 22 kcal/mol (Lazaridis et al. 2014) which is surprisingly close to our results despite the significantly different force fields and membrane models used.

Unlike the PMF of ARG9, which monotonically increases from bulk to the interior of bilayer, all the other peptides show a minimum at the interface region around 2 nm from the bilayer center. The SMTPs show a deeper minima ranging from −6.4 kcal/mol (TP1) to −7.9 kcal/mol (TP2, TP3), whereas the control peptides ONEG and DNEG only have a minimum of −2.5 and −3.4 kcal/mol, respectively. The presence of deep minima in the PMFs suggests SMTPs bind more strongly to the membrane interface. Electrochemical impedance spectroscopy (EIS) experiments (Lin et al. 2012) show that the fraction of peptide binding to 95:5 POPC:POPG membranes is 2×10^{-4} for TP2, and 2×10^{-6} for ONEG. The control peptide has a 100-fold weaker binding profile to the membrane compared to the SMTP. In Lin's work (Lin et al. 2012), the authors also observed that absolute binding free energies are higher. They found that the binding free energy of TP2 measured by equilibrium filtration method is about −3.0 kcal/mol and that for ONEG was estimated using the Membrane Protein Explorer tool to be about 1.0 kcal/mol. We believe this is because of the smaller molar fraction of POPG component used in the experiment. Generally, for cationic peptides, increasing the percentage of anionic lipids will lead to stronger binding to the membrane. For highly charged ARG9, we can see from our simulation results that the addition of 10 % POPG lowers the interfacial barrier by about 5 kcal/mol, compared to a pure zwitterionic phosphatidylcholine lipids (Hu et al. 2014).

Figure 3, center and far right panels, shows the enthalpic and entropic contributions to the total potentials of mean force; the profiles are zeroed in the bulk aqueous solution. For all peptides excluding ARG9, the enthalpic contribution to the potential of mean force confers the dominant stabilization energy in the interface region where the total pmf exhibits the global minima for all peptides. Moving away from the interface, in all cases, enthalpic contributions become unfavorable and ultimately contribute a destabilization effect to the overall free energetics of translocation. The entropy follows the reverse behavior of the enthalpy. At the interface, entropic contributions for all peptides excluding ARG9 are destabilizing. This is a consequence of the stronger binding of the peptides relative to ARG9, which shows no binding predilection. Peptides' strong binding most likely leads to more constrained system dynamics, with the system exploring less configurational space once the peptides are bound in place at the interface. In all the cases, as the peptides approach and then reside at the bilayer center, the general disruption of peptide structure is translated into a larger number of microstates accessible to the entire system, resulting in the fairly large entropic stabilization. The entropic stabilization is insufficient to dominate the larger destabilization enthalpic component, thus giving rise to the overall positive barriers in all cases. The large free energy penalty is related to the dehydration of highly solvated peptide inside the bilayer. (see more discussion in reference Hu et al. 2013) We compute the average number of water, choline, and phosphates present within a distance 0.67 nm of all peptide beads as a function of order parameter shown in Fig. 4. In all cases, the average number of water molecules present in the first solvation shell falls significantly from bulk water to the interior region of bilayer. Previously, we found that such difference is in agreement with the larger destabilization contribution arising from water (Hu et al. 2014). Opposite to the trend of water number change, the number of charged bead choline and phosphates increase along the path into the bilayer. We have shown that the interaction of peptide arginine residue with headgroups stabilize the peptide (Hu et al. 2013). It's important to notice that there

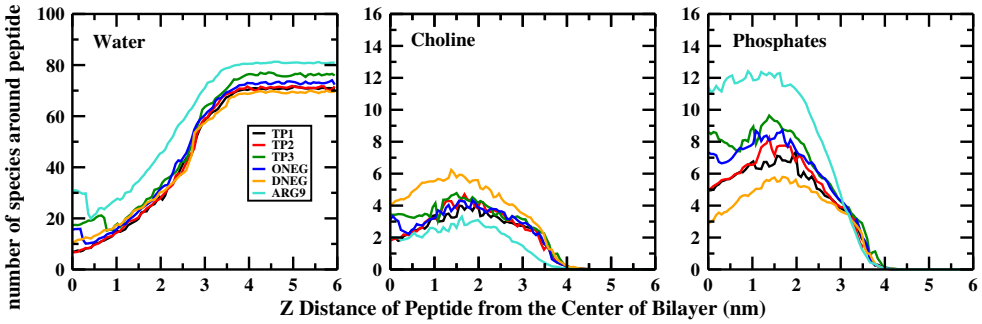

Fig. 4 Average number of water (water central bead name W), choline (bead name NC3) and phosphates (bead name PO4) present within 0.67 nm distance to all peptide beads, which we consider as the he first solvation shell of the peptide (Hu et al. 2014)

are more choline around negatively charged peptide, while more phosphates around positively charged peptide, and for water, the number is similar for them, except ARG9 which has three times charges than others.

Peptide Structural Features

The previous section's free energy results suggest that SMTPs have smaller barriers to translocation compared to control peptides. To further investigate the translocation process, we consider peptide and bilayer structure.

Along the translocation from bulk to center of the bilayer, we observe different behaviors for binding and non-binding peptides at the interface and interior of membrane. For all the peptides studied, we found the radius of gyration, R_g, is around 0.8 nm at the bulk water as shown in Fig. 5a. An increased R_g was observed near the interface region for all peptides except for ARG9. The radius of gyration increases about 0.1 nm for all the binding peptides, and there is no change for ARG9 which does not bind. The binding propensity of the SMTP peptides drives them to the bilayer-water interface. The increase of R_g at the interface is most likely a result of the disparate types of residues seeking to situate themselves in appropriate environments. The hydrophobic residues tend to bury deeper into the bilayer, while the charged and polar groups maintain interactions with polar headgroups and solvent. However, once bound to the membrane and moving past the interface, R_g decreases back to bulk values. When the peptides move toward the interior of the membrane, membrane is also deformed. The R_g decreases. This implies that a globular structure is preferred to reduce the deformation free energy cost. Interestingly, once the pore formed, a sharp increase of R_g was found in TP3, ONEG, and ARG9. These peptides span across the bilayer, with the polar and non-polar residues stabilized by the interaction with the headgroups and tails (see snapshots of center window win0 in Fig. 6).

Membrane Deformation

The PMFs in Fig. 3, left panel, show a decrease in the free energy barrier for TP3 and ONEG approaching the bilayer center. From the simulations, we see that this is because of the formation of pores manifested as generic deformations of the bilayer and inclusions of water and headgroups around the peptide as it resides in the bilayer

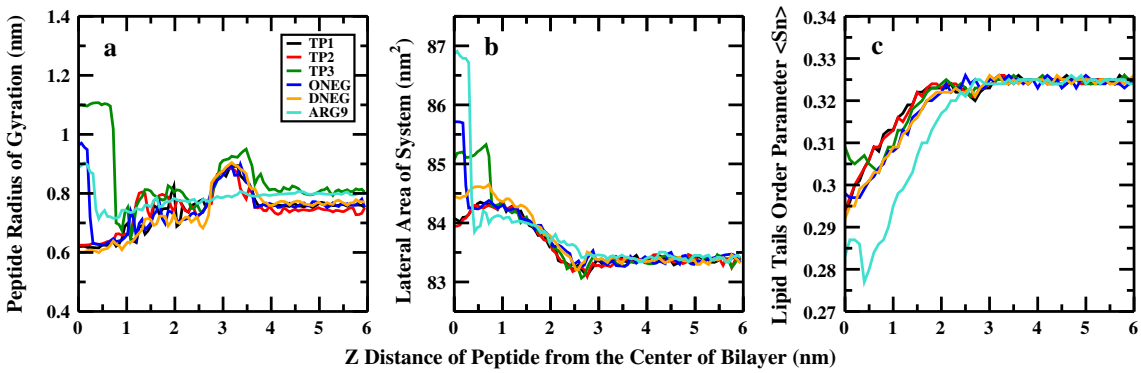

Fig. 5 The changes of (**a**) peptide radius of gyration, (**b**) area per lipid (**c**), and lipid tail average order parameters ⟨Sn⟩ along with peptide translocation

interior. However, we also observe pore formation for ARG9, but the free energy barrier is higher (see snapshots in Fig. 6).

We rationalize this by observing that for TP3 and ONEG, there are more hydrophobic residues, and the lipid core can stabilize these residues; the presence of hydrophobic residues in the peptide offsets polar group desolvation. However, ARG9 only contains cationic arginine residues. The lipid core will destabilize the peptide, since the large positive charge of the entire peptide is desolvated, and within the context of this force field, the deformation of the bilayer to provide a pore containing water and polar headgroup atoms is not sufficient to provide further stability to offset the desolvation. We will address aspects of bilayer structural perturbations further below.

In Fig. 7, we compute lipid headgroup, tail, and total lipid density along the bilayer cross section. Red to orange coloration indicates high density, while blue to white indicates low density. Figure 7 shows that when ARG9 resides at bilayer center, lipid headgroups are associated with the peptide and present in a region of the bilayer that is considered the hydrophobic core region. There are no

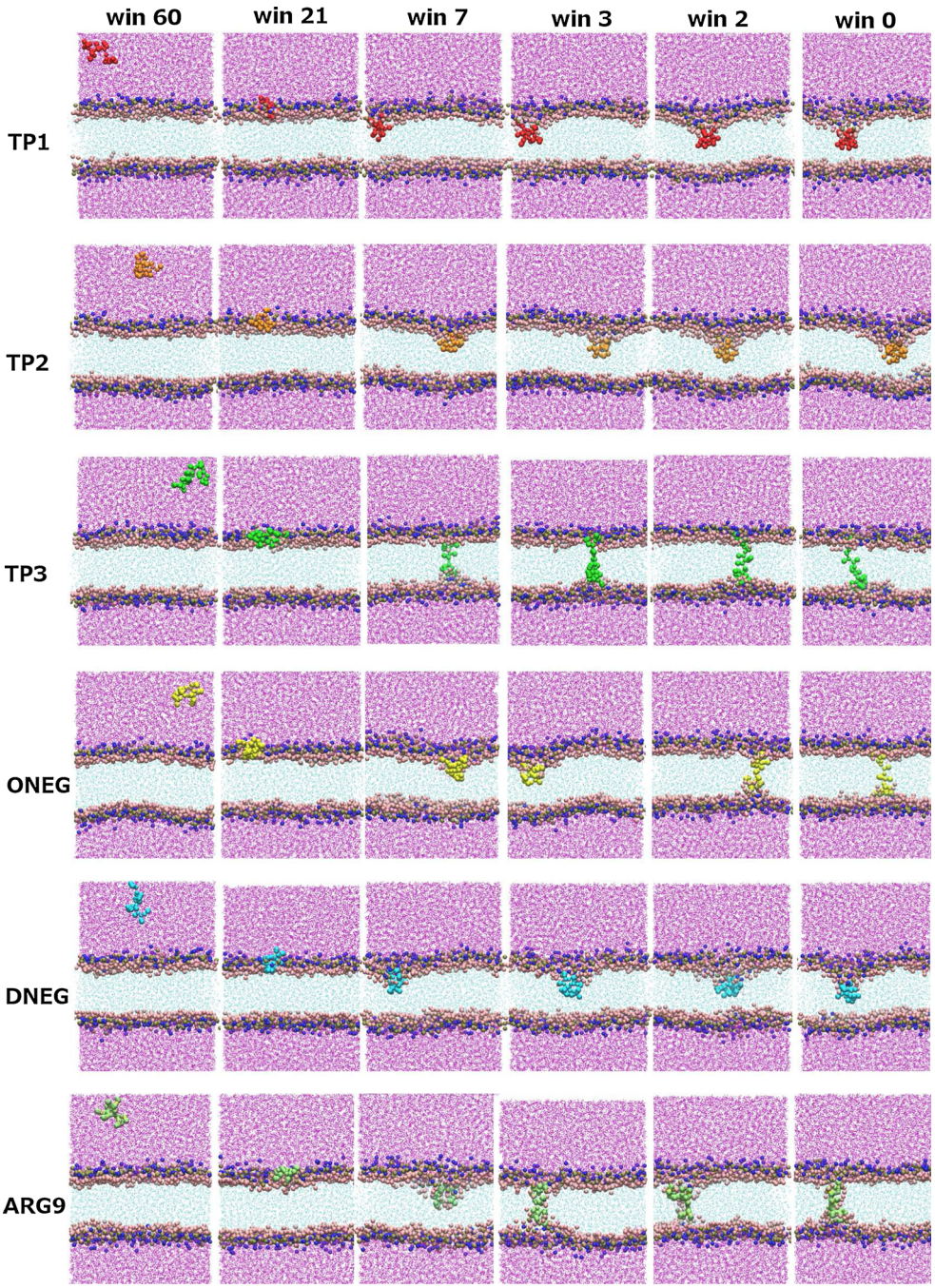

Fig. 6 Representative snapshots of (*panels* in each row) peptide TP1, TP2, TP3, ONEG, DNEG, and ARG9 translocation from bulk into the center of the model 90:10 POPC:POPG lipid bilayers. The peptides are restrained at (*panels* in each column) bulk water (win60), interface (win21), interior of membrane (win7, win3, win2 represent z-distance of 0.7, 0.3, and 0.2 nm to the bilayer core), and center of the bilayer (win0). Lipid headgroups and peptides are shown as spherical balls

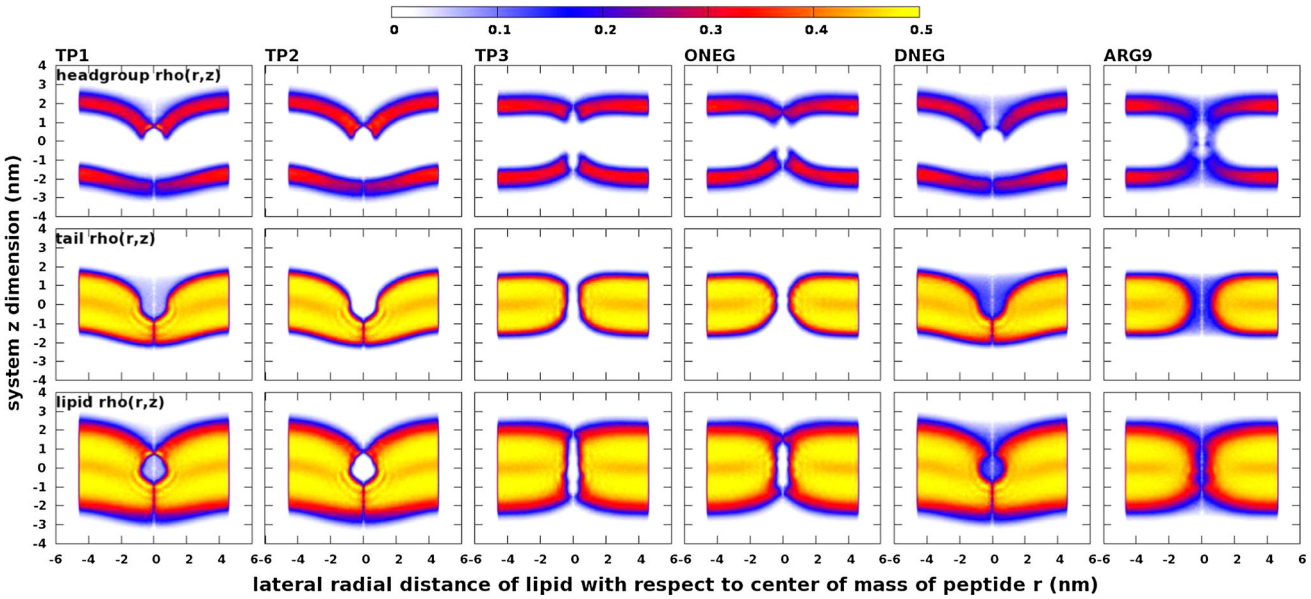

Fig. 7 Two-dimensional density profile $\rho(r, z)$ of the center window (win0) for (*top panels*) lipid headgroup, lipid tails, and the whole lipid bilayers in each peptide system as a function of the lateral radial distance with respect to the center of mass of the peptide (r), and the system z-dimension. TP1, TP2, and DNEG only have membrane water defects, but TP3, ONEG and ARG9 form water pores. The pore structures in TP3 and ONEG are different with ARG9. The former one is known as hydrophobic pore, and the latter one is considered as hydrophilic pore

headgroups present in ONEG and TP3. Usually, membrane pore can be divided into three categories: hydrophilic pore, hydrophobic pore, and vapor pore (Notman et al. 2008). A hydrophilic pore consists of water and lipid molecules from both the upper and lower leaflet, and the membrane hydrophilic headgroups in the local pore region reorient to the rim/edge of the pore, shielding the hydrocarbon tails from the solution and allowing small hydrophilic solute to pass through. In a hydrophobic pore, the hydrocarbon tails are directly exposed to the water, with few or no headgroups reoriented. Vapor pore is similar lipid structure as hydrophobic, but there is no water present inside a vapor pore. Thus, our result show that ARG9 forms a hydrophilic pore, while TP3 and ONEG form a hydrophobic pore (see snapshots in SI figure S13). TP1, TP2, and DNEG do not form pores, in our definition but rather show membrane deformation defects. Thus, we will not speak about them in the context of pore formation. In the hydrophilic pore, the headgroup atoms reorient to form the rim of the pore and strongly interact with the polar residues of ARG9 and stabilize ARG9. From the edge of the $\rho(r, z)$ of the tail groups, we roughly estimate the pore size in TP3, ONEG, ARG9 are about 0.5, 0.5, and 1.0 nm (see the middle row in Fig. 7). TP3 tends to form pore at a shallower depth, the first pore window are found at a depth of 0.7 nm, while ONEG is found at 0.2 nm, and ARG9 is found at 0.3 nm. From a 1,000 ns free molecular dynamics simulation, we see that all the polar residue prefer to stay at the headgroup region, however, the non-polar residue penetrate deeper inside to interact with the non-polar tails (see Fig. 2). These pores are stable, and they do not lead to membrane rupture. We note that the formation of pores associated with peptide translocation is often suggested in the literature (Laettig-Tuennemann et al. 2011; Huang and García 2013; Hu et al. 2014). Dye leakage observations during peptide translocation are one assay used to assess the formation of pores. Our results are consistent with experimental indications there can be little or no dye leakage (Marks et al. 2011). Due to the limitations of experiment, the ability to detect dye leakage is limited by the size of probe. The routinely used analytes are fluorescent dyes (for example TAMRA), citrate chelated Tb^{3+}, dextrans, all having diameters of 1.0 nm or more (Lin et al. 2012). Considering the size of the pore, which is less than 1.0 nm, even if a pore is stable (usually pore in lipid is known as transient pore), it will only allow certain sizes of dye or ions to pass through. In TP3 and ONEG, the pore size is smaller than the probe size, perhaps suggesting a reason why experimentally no dye leakage is observed (Marks et al. 2011; Lin et al. 2012).

Along the penetration path to the center of bilayer, the lateral area of the system expands after the peptides approach to the interface. A significant increase occurs when a pore is finally formed in the system. However, this difference is relatively small. The area is only changed by 2–4 %. Even for ARG9, where there is a 1.0-nm pore

formed in the membrane, the lateral area of the system only increases by 4 %. In this infinite dilute system, there is no obvious membrane rupture, but in a concentrated peptide system, this change will may not be ignored.

From the snapshots in Fig. 6, all the peptides cause membrane deformation. To explore the extent of such deformation, we have calculated orientational-order parameter for the membrane tails in all cases by using equation $\langle S_n \rangle \leq \frac{1}{2}(3\cos^2\theta - 1) >$ where θ is the angle between the bond of the tail and the bilayer normal in the range 0–180 °, and $\langle \cdots \rangle$ denotes an average over all values of S_n. The range of S_n is from -0.5 to 1. The value of 1 corresponds to perfect nematic order with bilayer norm, 0 means randomly oriented, and -0.5 means the bonds confined to the plane perpendicular to bilayer normal. In Fig. 5, we plot the average order parameters $\langle S_n \rangle$ as a function of bilayer depth. The result shows that for all peptides, the bilayer becomes disordered when peptide penetrates deeper inside the membrane. When there are more hydrophilic residues such as ARG9, the disorder of the membrane is more significant. Such disorder enhances the membrane deformation and lessens effects associated with desolvation of peptide.

Discussion and Summary

We have presented results of Martini coarse-grained force field simulations to estimate the potentials of mean force for a series of recently screened spontaneous membrane-translocating peptides, SMTPs. We consider the diffusive process of peptide translocation along an order parameter describing the z-distance separation between the centers of mass of the peptide and the bilayer. We consider model bilayer composed of POPC and POPG, the latter providing the anionic component as used in experimental studies. In accordance with a plethora of experimental observations, we observe a significant barrier for translocation in the case of the canonical cationic CPP ARG9. This suggests an energy-mediated, non-spontaneous mechanism of internalization for this peptide. In the case of the TP1, TP2, and TP3 peptides, the computed potentials of mean force are systematically lower relative to the ARG9 case. Though the barriers predicted by the simulations, on the order of 20 kcal/mol, are still rather large to recapitulate the experimental kinetics of internalization, we emphasize that the qualitative trend of reduction of barrier heights is a significant result. Furthermore, in comparing the translocation process in the presence and absence of a pathway that accommodates the formation of a long-lived, stable pore, we find, as in previous studies, that the pore-forming pathway is the lower free energy pathway (lowered by an amount of 90 kJ/mol). In this sense, the coarse-grained model further reinforces the conclusions of the all-atom simulations (Huang and García 2013). Nevertheless, the high barriers predicted contradict the efficient internalization of this peptide into cells and model giant plasma membrane vesicles (GPMV) (Saalik et al. 2011). This suggests several areas of concern regarding force field calculations and the interpretation of such calculations. First, due to the lack of atomistic detail in CG model, the current force field may not reflect actual energy scales found in nature (but this argument can be applied to all empirical force fields). Furthermore, system size effects may contribute to free energetics of internalization. As shown by Hu et al. (2013), system size effects are significant in all-atom force field-based calculations of potentials of mean force for arginine translocation in model PC bilayers. Of course, the effects of system size are difficult to assess, particularly with the coarse-grained models studied here as the reaction coordinate chosen a priori become degenerate when used in systems in conjunction with larger lateral system dimensions. Furthermore, we neglect contributions from the diffusion constant profile of the peptides along the order parameter, but based on previous work in our laboratory and by others, diffusion constants generally are lower in the bilayer environment than in bulk aqueous solutions. This would tend to increase translocation timescales related to our predicted potentials of mean force. Decomposition of the PMFs indicates that though there is a substantial entropic stability when the peptides reside at bilayer center, barriers as predicted from these force field-based studies are largely determined by enthalpic (potential energy) interactions. We note that in the case of TP3, a substantial hydrophilic pore is formed, where lipid headgroup atoms are found to associate with charged and polar residues of the peptide as the peptide resides at the center of the bilayer. This pore confers roughly 5 kcal/mol stability to the peptide as the bilayer center. In fact, TP3 exhibits a maximum in the potential of mean force about 0.8 nm from the bilayer center, where the pore is formed. Following pore formation, the potential of mean force decreases. Relative to the bulk aqueous environment, the free energy of the peptide at bilayer center is only 5 kcal/mol higher. The notion of pores of various kinds has been offered in the experimental literature as a possible mechanistic requirement for translocation of certain types of peptides. In the case of TP1 and TP2, we find that no pores are formed, and the membrane undergoes an elastic deformation to accommodate the peptide at positions interior in the membrane. We note that the binding of the SMTPs is critically dependent on the mix of hydrophilic and hydrophobic residues that constitute the amino acid motif/sequence of these peptides. Analysis of distributions of the absolute positions of individual amino acid residues suggests that the

preferential binding of the peptides at the interface is facilitated by the presence of hydrophobic residues that can penetrate further into the bilayer. These residues then can accommodate the peptide as it moves into the bilayer center, with the more polar and charged groups, such arginine residues, still interacting with the polar headgroups and water in the interfacial regions.

The spacing between arginine and hydrophobic residues appears to be one critical factor in defining peptide translocation characteristics. The conserved specific motif ΦR$\Phi\Phi$R reduces the free energy barrier significantly for peptide translocation into the membranes studied here. For future drug delivery peptide design, this motif may be a critically important moiety to be included in consideration of peptide sequence space. Generally, a set of hydrophobic residues helps stabilize the inner bilayer states, and arginine residues interact with the phosphates and must operate in a way that allows binding and unbinding with the interface to allow entry into the bilayer. Thus, it is important to investigate the correlation of this motif with the lipid type, the thickness of bilayer, and other membrane characteristics in the future. The type of lipid usually affects the peptide interfacial binding. A tighter binding will trap the peptides at the membrane interface and make it more difficult to transit from the interfacial minimum and move to inner membrane locations. Different thicknesses of the bilayer may require either extended or shorter length of the hydrophobic or hydrophilic spacing in the motif. Such studies are timely and ongoing.

Acknowledgments The authors acknowledge support from the National Science Foundation (CAREER:MCB:1149802). Computational resources are acknowledged via support from National Institutes of Health COBRE:P20-RR015588 in the Chemical Engineering Department and COBRE:P20-RR017716 in the Department of Chemistry and Biochemistry at the University of Delaware. S. P. thanks N. Patel for fruitful discussion and encouragement for the duration of this work.

References

Bangel U (ed) (2006) Handbook of cell penetrating peptides, 2nd edn. CRC, Boca Raton

Bechara C, Sagan S (2013) Cell-penetrating peptides: 20 years later, where do we stand? FEBS Lett 587:1693–1702

Berendsen HJC, Postma JPM, Gunsteren WFV, DiNola A, Haak JR (1984) Molecular dynamics with coupling to an external bath. J Chem Phys 81:3684–3690

Cruz J, Mihailescu M, Wiedman G, Herman K, Searson P, Wimley K, Hristova William (2013) A membrane-translocating peptide penetrates into bilayers without significant bilayer perturbations. Biophys J 104(11):2419–2428

DeJong DH, Singh G, Bennett WFD, Arnarez C, Wassenaar TA, Schäfer LV, Periole X, Tieleman DP, Marrink SJ (2013) Improved parameters for the martini coarse-grained protein force field. J Chem Theory Comput 9(1):687–697

Freites JA, Tobias DJ, White SH (2006) A voltage-sensor water pore. Biophys J 91(11):L90–L92

Green M, Loewenstein PM (1988) Autonomous functional domains of chemically synthesized human immunodeficiency virus tat trans-activator protein. Cell 55:1179–1188

He J, Hristova K, Wimley WC (2012) A highly charged voltage-sensor helix spontaneously translocates across membranes. Angew Chem Int Ed Engl 51(29):7150–7153

He J, Kauffman WB, Fuselier T, Naveen SK, Voss TG, Hristova K, Wimley WC (2013) Direct cytosolic delivery of polar cargo to cells by spontaneous membrane-translocating peptides. J Biol Chem. doi:10.1074/Jbc.M113.488312

Hess B, Bekker H, JCBerendsen H, GEMFraaije J (1997) LINCS: a linear constraint solver for molecular simulations. J Comput Chem 18(12):1463–1472

Hu Y, Ou S, Patel S (2013) Free energetics of arginine permeation into model dmpc lipid bilayers: coupling of effective counterion concentration and lateral bilayer dimensions. J Phys Chem B 117: 11641–11653

Hu Y, Liu X, Sinha SK, Patel S (2014) Translocation thermodynamics of linear and cyclic nonaarginine into model dppc bilayer via coarse-grained molecular dynamics simulation: Implications of pore formation and nonadditivity. J Phys Chem B 118(10): 2670–2682

Huang K, García AE (2013) Free energy of translocating an arginine-rich cell-penetrating peptide across a lipid bilayer suggests pore formation. Biophys J 104(2):412–420

Järver P, Langel Ü (2006) Cell-penetrating peptides—a brief introduction. Biochim Biophys Acta 1758:260–263

Jiao CY, Delaroche D, Burlina F, Alves ID, Chassaing G, Sagan S (2009) Translocation and endocytosis for cell-penetrating peptide internalization. J Biol Chem 284(49):33957–33965

Kosuge M, Takeuchi T, Nakase I, Jones AT, Futaki S (2008) Cellular internalization and distribution of arginine-rich peptides as a function of extracellular peptide concentration, serum, and plasma membrane associated proteoglycans. Bioconjug Chem 19(3):656–664

Kumar S, Rosenberg JM, Bouzida D, Swendsen RH, Kollman PA (1992) The weighted histogram analysis method for free-energy calculation s on biomolecules. i. The method. J Comp Chem 13(8):1011–1021

Laettig-Tuennemann G, Prinz M, Hoffmann D, Behlke J, Palm-Apergi C, Morano I, Herce HD, Cardoso MC (2011) Backbone rigidity and static presentation of guanidinium groups increases cellular uptake of arginine-rich cell-penetrating peptides. Nature Commun 2:1–6

Lazaridis T, III JML, PeBenito L (2014) Implicit membrane treatment of buried charged groups: application to peptide translocation across lipid bilayers. Biochim Biophys Acta. http://dx.doi.org/10.1016/j.bbamem.2014.01.015

Lin J, Motylinski J, Krauson AJ, Wimley WC, Searson PC, Hristova K (2012) Interactions of membrane active peptides with planar supported bilayers: an impedance spectroscopy study. Langmuir 28(14):6088–6096

Lundberg P, Langel Ü (2003) A brief introduction to cell-penetrating peptides. J Mol Recognit 16:227–233

Marks JR, Placone J, Hristova K, Wimley WC (2011) Spontaneous membrane-translocating peptides by orthogonal high-throughput screening. J Am Chem Soc 133(23):8995–9004

Marrink SJ, Vries AHD, Mark AE (2004) Coarse grained model for semiquantitative lipid simulations. J Phys Chem B 108(2): 750–760

Monticelli L, Kandasamy SK, Periole X, Larson RG, Tieleman DP, Marrink SJ (2008) The martini coarse-grained force field: extension to proteins. J Chem Theory Comput 4(5):819–834

Notman R, Anwar J, Briels W, Noro MG, den Otter W (2008) Simulations of skin barrier function: free energies of

hydrophobic and hydrophilic transmembrane pores in ceramide bilayers. Biophys J 95(10):4763

Pavan S, Berti F (2011) Short peptides as biosensor transducers. Anal Bioanal Chem 402:3055–3070

Saalik P, Niinep A, Pae J, Hansen M, Lubenets D, Langel U, Pooga M (2011) Penetration without cells: membrane translocation of cell-penetrating peptides in the model giant plasma membrane vesicles. J Control Release 153(2):117–125

Schmidta N, Mishrab A, Laia GH, Wong GC (2010) Arginine-rich cell-penetrating peptides. FEBS Lett 584:1806–1813

Schow EV, Freites JA, Cheng P, Bernsel A, von Heijne G, White SH, Tobias DJ (2011) Arginine in membranes: the connection between molecular dynamics simulations and translocon-mediated insertion experiments. J Membr Biol 239(1–2):35–48

Shin MC, Zhang J, Min KA, Lee K, Byun Y, David AE, H He VCY (2013) Cell-penetrating peptides: achievements and challenges in application for cancer treatment. J Biomed Mater Res A 00:00–00

Tunnemann G, Ter-Avetisyan G, Martin RM, Stockl M, Herrmann A, Cardoso MC (2009) Live-cell analysis of cell penetration ability and toxicity of oligo-arginines. J Biol Chem 14(4):469–476

Walrant A, Matheron L, Cribier S, Chaignepain S, Jobin ML, Sagan S, Alves ID (2013) Direct translocation of cell-penetrating peptides in liposomes: a combined mass spectrometry quantification and fluorescence detection study. Anal Biochem 438(1):1–10

Yesylevskyy SO, Schäfer LV, Sengupta D, Marrink SJ (2010) Polarizable water model for the coarse-grained martini force field. PLoS Comput Biol 6(6):e1000810

Zorko M, Langel U (2005) Cell-penetrating peptides: mechanism and kinetics of cargo delivery. J Mol Recognit 57:529–545